ACS OMEGA

Article

Cite This: ACS Omega 2019, 4, 16068−16079

http://pubs.acs.org/journal/acsodf

Synthesis of Two Mononuclear Schiff Base Metal (M = Fe, Cu) Complexes: MOF Structure, Dye Degradation, H_2O_2 Sensing, and DNA Binding Property

Mithun Kumar Ghosh,[†] Sayantan Pathak,[‡] and Tanmay Kumar Ghorai*[,†]

[†]Nanomaterials and Crystal Designing Laboratory, Department of Chemistry, Indira Gandhi National Tribal University, Amarkantak, Madhya Pradesh 484887, India

[‡]Department of Chemistry, University of Gour Banga, Malda, West Bengal 732103, India

Supporting Information

ABSTRACT: O-Vanillin and ethylenediamine were used for the synthesis of *N*,*N*′-bis(O-vanillinidene)ethylenediamine (O-VEDH$_2$) Schiff base ligand, which was characterized by UV−visible and ^{1}H NMR spectroscopy. The Schiff base ligand O-VEDH$_2$ has been employed to synthesize novel $[C_{18}H_{22}FeN_2O_6]NO_3$ (**1**) and $C_{18}H_{16}CuN_2O_5$ (**2**) complexes by the simple slow evaporation method. The single crystals were characterized by X-ray crystallography, as well as Fourier-transform infrared and UV−visible spectroscopy techniques. Complexes **1** and **2** crystallize in monoclinic and orthorhombic space groups with *P*121/*n*1 (14) and *Pnma* (62) point groups, respectively, and both show metal−organic frameworks like structures. Complexes **1** and **2** have optical band gaps of 4.1 and 2.9 eV, respectively, indicating their semiconducting properties. The dye degradation activity and H_2O_2 sensing of the complexes **1** and **2** were determined in different conditions. The photocatalytic test was performed in the presence of sunlight, methylene blue (MB), and complexes **1** and **2**. An interesting result was obtained that complex **2** has degradation ability against MB and the rate constant (K) is 5.46×10^{-5} s^{-1}, whereas complex **1** has H_2O_2 sensing properties. Both complexes are bound to Calf-thymus DNA by intercalation binding mode, and binding constants (K_b) of complexes **1** and **2** are 3.77×10^3 and 1.49×10^4 M^{-1}, respectively.

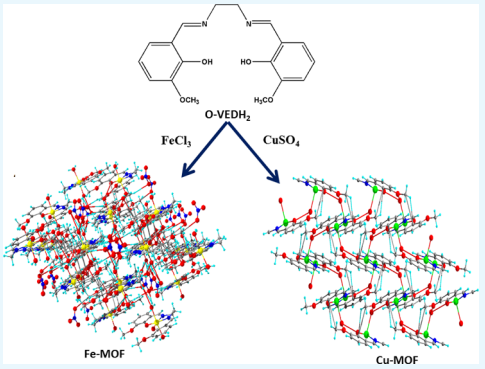

INTRODUCTION

The Schiff base metal complexes are used extensively in the field of materials science, including catalyst, supramolecular chemistry, anticancer, antimicrobial, antioxidants, electrochemistry, photocatalysts, DNA binding, and energy materials.[1−14] In general, the Schiff base can assemble the metal ions to develop metal−organic framework (MOF) compounds and shows different properties like dye adsorption, sensing, semiconductor, and biological properties.[15−23]

In recent years, researchers from around the world have been working to synthesize metal−organic framework complexes to promote the degradation or adsorption of dyes and to eliminate the dyes from chemically contaminated water.[24−27] Because most of the synthetic dyes were used in a wide range of industries, such as paper, plastics, leather tanneries, food technology, and cosmetics,[28,29] waste dyes are discharged into rivers and ponds, thereby contaminating the water. These dye contaminants can cause allergies, skin irritation, liver damage, kidney damage, and also central nervous system disorders in humans and animals.[30] Currently, Yang et al. reported that three-dimensional (3D)-pillared layer copper(II) MOFs have been used for dual purposes, i.e., dye adsorption and separation.[31]

Nowadays, MOFs have often been used as different types of sensing materials, i.e., H_2O_2 sensing. Reactive oxygen species like H_2O_2 are nontoxic but produce free radicals such as superoxide anion ($O_2^{\bullet-}$) and hydroxyl radical ($^{\bullet}OH$) at the time of decomposition, which plays an important role for the initiation of cancer, autoimmunity, neurodegenerative disorders, etc.[32−34] Hydrogen peroxide is widely used in the food, cosmetic, pharmaceutical, paper, and chemical industries.[35,36] Therefore, it is necessary to detect H_2O_2 for the healthy life of humans and animals. In the last few years, scientists have developed iron- and copper metal-based MOFs and reported variable sensing applications, i.e., fluorescent, luminescent, photocatalytic, and polar aliphatic volatile organic compounds.[37−41]

MOFs, as well as various Schiff base ligands, play an important role in bioapplications. The effective anticancer drugs have an active site primarily targeted to bind the DNA of the cancer cell, reducing the activity of the cancer cell and resulting in cell death.[42−44] Anticancer drugs interact with cancer cell DNA through electrostatic, intercalative, or groove binding, which

Received: July 22, 2019
Accepted: September 3, 2019
Published: September 17, 2019

DOI: 10.1021/acsomega.9b02268
ACS Omega 2019, 4, 16068−16079

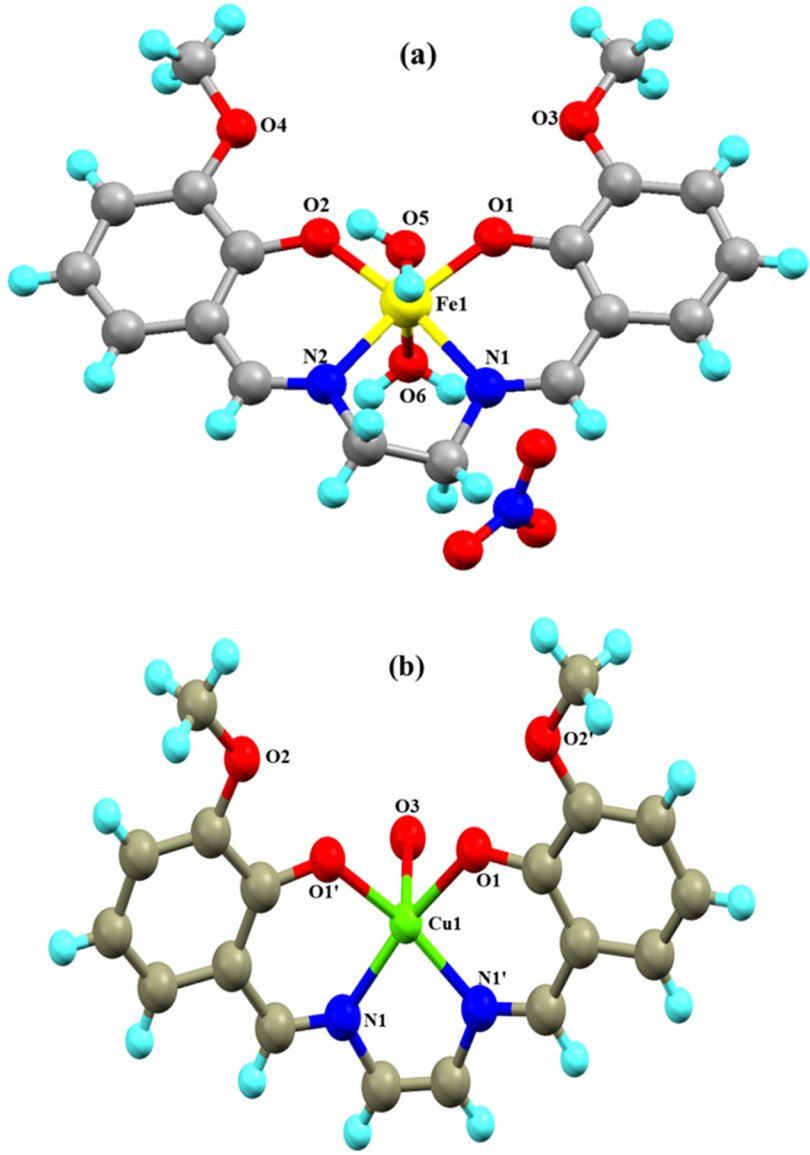

Figure 1. (a) Complex **1** and (b) complex **2**.

depends on the binding modes of anticancer drugs.[25,45−47] The Schiff base ligands and the corresponding metal complexes have the active site that interacts with the DNA of the cancer cell.[48,49] Recently, metal−organic framework systems have been used in biomedicine, as reported by Chen et al.[50,51]

In this study, we have designed and synthesized *N*,*N*′-bis(O-vanillinidene)ethylenediamine (O-VEDH$_2$) Schiff base ligand and employed it for the synthesis of new $[C_{18}H_{22}FeN_2O_6]NO_3$ (**1**) and $C_{18}H_{16}CuN_2O_5$ (**2**) complexes. The main aim of our research work is to synthesize transition-metal complexes using synthesized Schiff base ligand and study their multifunctional applications, i.e., dye degradation, H_2O_2 sensing, and DNA binding activity. The Schiff base ligand is characterized by UV−visible and ^{1}H NMR spectroscopies. From optical measurements, complexes **1** and **2** have energy band gaps of 4.1 and 2.9 eV, respectively, and show semiconductor property. Complex **1** can actively sense H_2O_2, whereas complex **2** has no such sensing ability. On the other hand, complex **2** has photocatalytic activity; it degrades methylene blue (MB) and the rate constant (K) is 5.46×10^{-5} s^{-1}, but complex **1** has no photocatalytic activity. Both the complexes bind to Calf-thymus DNA (CT-DNA) through intercalation binding mode, and their binding constants (K_b) were found to be 3.77×10^3 and 1.49×10^4 M^{-1}, respectively.

RESULTS AND DISCUSSION

Structural Description. Complexes **1** and **2** crystallize in monoclinic and orthorhombic space groups with $P121/n1$ and *Pnma*, respectively, as shown in Figure 1. The phase data of the complexes are shown in Table 1, and the selected interatomic distances and angles are listed in Table 2. Both complexes have butterfly-like structures. Complex **1** was coordinated by two nitrogen atoms, N(1) and N(2), and two hydroxyl oxygen atoms, O(1) and O(2), of O-VEDH$_2$ moiety and two oxygen atoms, O(5) and O(6), of two water molecules and form an octahedral geometry. Two water molecules are present in the axial position of complex **1**. The oxidation state of the metal ion is stabilized by nitrate ion (NO_3^-) (surrounding the complex) and the corresponding protonated oxygen atom in complex **1**, whereas complex **2** was coordinated by two nitrogen atoms, N(1) and N(1)a, and hydroxyl oxygen atoms, O(1) and O(1)a, from one O-VEDH$_2$ moiety and one oxygen (O_3) atom and

DOI: 10.1021/acsomega.9b02268
ACS Omega 2019, 4, 16068−16079

Table 1. Phase Data of Complexes 1 and 2[a,b,c,d]

parameter	complex 1	complex 2
formula	$[C_{18}H_{22}FeN_2O_6]NO_3$	$C_{18}H_{16}CuN_2O_5$
formula weight (g/mol)	480.2 g/mol	403.8 g/mol
temperature (K)	273 K	99 K
wavelength	0.71073 Å	0.71073 Å
crystal system	monoclinic	orthorhombic
space group	*P*121/*n*1 (14)	*Pnma* (62)
unit cell dimensions *a*, *b*, *c* (Å)	*a* = 11.8135(2), *b* = 13.3278(1), *c* = 13.8168(2)	*a* = 9.212(2), *b* = 24.643(5), *c* = 7.363(2)
α, *β*, *γ* (°)	*α* = 90, *β* = 111.607(2), *γ* = 90	*α* = 90, *β* = 90, *γ* = 90
V (Å^3)	2022.56(6)	1671.5(7)
Z	4	1
density (g/cm^3)	1.577	0.411
radiation type	Mo K*α*	Mo K*α*
μ (mm^{-1})	6.504	0.335
absorption correction	multiscan absorption correction	multiscan absorption correction
T_{min}, T_{max}	0.295, 1.00	0.571, 0.733
R_{int}	0.029	0.0878
θ (max) (Å^{-3})	71.360	24.996
refinement $R[F^2 > 2\sigma(F^2)]$, $wR(F^2)$, *S*	0.0502(3642), 0.1362(3879), 1.043	0.0568(1411), 0.1556(1496), 1.074
goodness of fit on F^2	1.041	1.052
no of reflections	3879	1496
no of parameters	284	122
data completeness	0.986	0.995

[a] $R1 = \sum(||F_o| - |F_c||)/\sum|F_o|$. [b] $wR2 = [\sum[w(F_o^2 - F_c^2)^2]/\sum w[(F_o^2)^2]]^{1/2}$. [c] $S = [\sum[w(F_o^2 - F_c^2)^2]/(n - p)]^{1/2}$. [d] $w = 1/[\sum^2(F_o^2) + (m*p)^2 + n*p]$, $p = [\max(F_o^2,0) + 2*F_c^2]/3$, *m* and *n* are constants.

Table 2. Selected Bond Distances (Å) and Bond Angles (°) for Complexes 1 and 2[a]

complex 1		complex 2	
atoms 1,2	*d* 1,2 (Å)	atoms 1,2	*d* 1,2 (Å)
Fe1−O1	1.882(16)	Cu1−N1/N1′	1.942(45)
Fe1−O2	1.866(21)	Cu1−O1/O1′	1.932(28)
Fe1−O5	2.316(13)	Cu1−O3	2.330(28)
Fe1−O6	2.088(26)		
Fe1−N1	2.094(26)		
Fe1−N2	2.075(27)		
atoms 1,2,3	angle 1,2,3 (°)	atoms 1,2,3	angle 1,2,3 (°)
O1−Fe1−O5	89.57(8)	O1−Cu1−O1′	90.48(16)
O1−Fe1−O2	101.45(8)	O1′−Cu1−O3	98.47(11)
O1−Fe1−O6	93.26(9)	O1−Cu1−O3	98.42(11)
O1−Fe1−N1	88.99(8)	O1−Cu1−N1	92.30(15)
O1−Fe1−N2	168.06(9)	O1−Cu1−N1′	166.99(18)
O2−Fe1−O5	92.04(8)	O1′−Cu1−N1′	92.30(15)
O2−Fe1−O6	91.91(9)	O1′−Cu1−N1	167.01(18)
O2−Fe1−N1	169.56(9)	N1−Cu1−O3	93.67(17)
O2−Fe1−N2	89.63(9)	N1′−Cu1−O3	93.73(17)
O6−Fe1−O5	174.60(9)	N1′−Cu1−N1	82.3(3)
O6−Fe1−N1	87.28(10)		
N1−Fe1−O5	88.17(8)		
N2−Fe1−O5	85.57(9)		
N2−Fe1−O6	90.77(10)		
N2−Fe1−N1	79.98(9)		

[a] Symmetry codes: primed atoms are related by symmetry $-x + 1$, *y*, $-z$.

Table 3. Bond Valence Sums[b] **for Complexes 1 and 2**[a]

	complex 1		complex 2	
atom	Fe(II)	Fe(III)	Cu(II)	Cu(I)
Fe1	3.29	<u>3.14</u>		
Cu1			<u>2.01</u>	1.76

[a] The oxidation state of a particular atom is the nearest integer to the underlined value. [b] The underlined value is the closest to the charge for which it was calculated.

developed square pyramidal structure. The oxidation states of the complexes **1** and **2** are found to be 3+ and 2+, which was also confirmed by the bond valence sum (BVS) calculation shown in Table 3.[52] The bond lengths between the metal-oxygen and nitrogen of the Schiff base ligand of both complexes are attached through their normal modes of coordination, i.e., for complex **1**, Fe1−O1, Fe1−O2, Fe1−O5, Fe1−O6, Fe1−N1, and Fe1−N2 are found to be 1.882(16), 1.866(21), 2.316(13), 2.088(26), 2.094(26), and 2.075(27) Å, respectively, and for complex **2**, Cu1−N1/N1′, Cu1−O1/O1′, and Cu1−O3 are found to be 1.942(45), 1.932(28), and 2.330(28) Å, respectively. The intra- and intermolecular H-bonds of complex **1** H5A−O9, H6A−O4, H6A−O9, O1−H6B, H5B−O4, O5−H6B, O5−H6A, O6−H5A, O2−H6A, H6A−N3, H6A−O7, N1−H5A, N2−H6A, N1−H6B, N2−H5A, N2−H5B, O2−H5B, O7−H6B, H6B−N3, H6B−O9, O8−H6B, N3−H6B, N3−H6A, and H6A−O8 are found to be 4.669(48), 4.986(29), 4.382(48), 3.006(17), 4.572(21), 4.554(15), 4.558(13), 4.537(23), 3.045(19), 3.398(29), 3.185(54), 2.793(28), 2.738(23), 2.667(21), 2.771(26), 3.028(30), 2.732(14), 2.851(57), 2.655(29), 3.692(45), 4.753(35), 3.686(26), 2.764(26), and 3.927(39) Å, respectively, as shown in Figure 2a, whereas complex **2** has no intra- and intermolecular H bonding. Figures 2b and 3a represent van der Waals interaction between complexes **1** and **2**, and their corresponding van der Waals bond lengths are shown in Table 4, which stabilized the complexes. Complex **2** has an asymmetric unit, as shown in Figure 3b, whereas complex **1** has no asymmetric unit. The most interesting feature was obtained that both the complexes have built metal−organic frameworks (MOFs) fabricated through Schiff base ligands

DOI: 10.1021/acsomega.9b02268
ACS Omega 2019, 4, 16068−16079

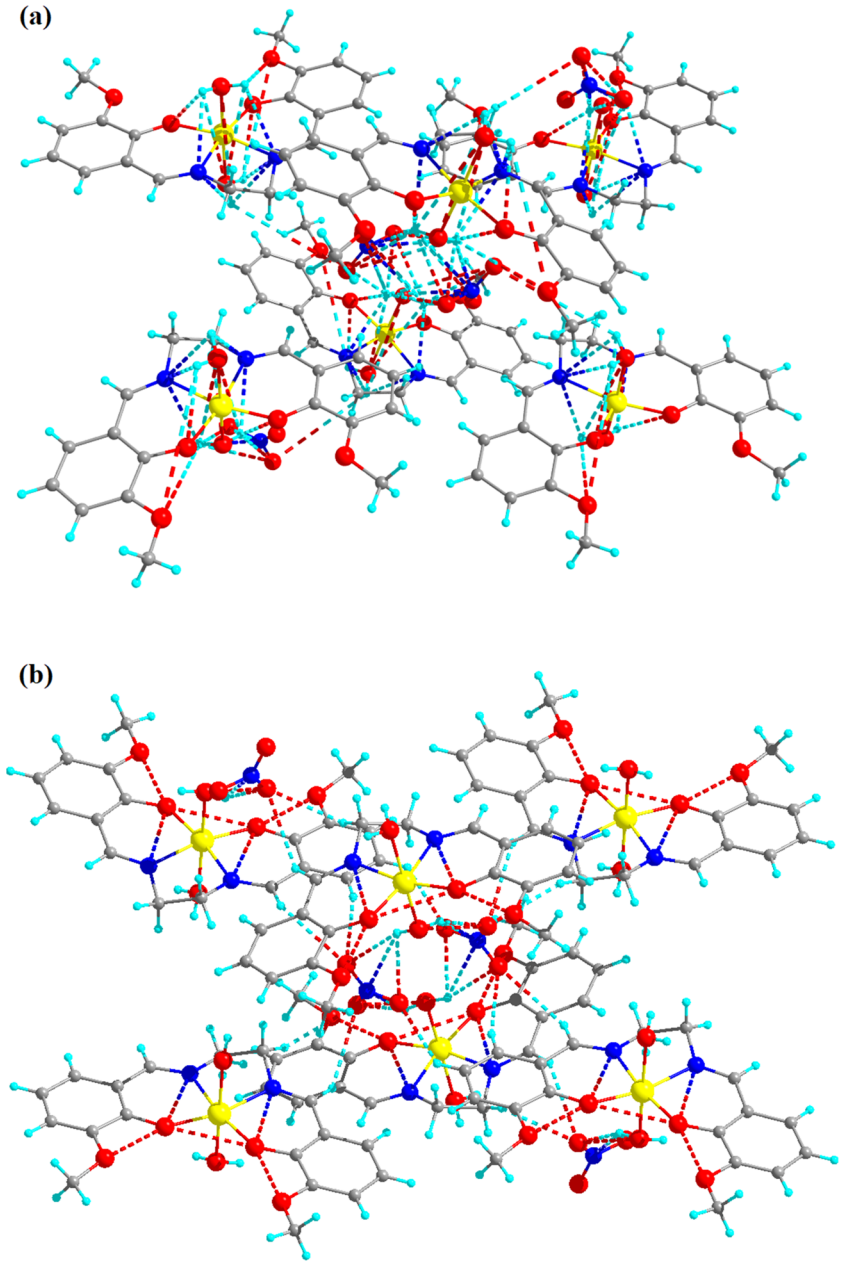

Figure 2. (a) Intra- and intermolecular H-bonding and (b) van der Waals interaction of complex **1**.

linked to the entire two-dimensional net and a 3D layer framework for **1** and **2**, as shown in Figure 4a,b, respectively.

Optical Properties. To explain the conductivity of the isolated complexes, the optical band gap energy of the complexes was calculated by the Tauc formula according to eq 1

$$(\alpha h\upsilon)^n = A(h\upsilon - E_g) \quad (1)$$

where α denotes the absorption coefficient, which is calculated as $\alpha = (2.303 \times \text{absorption})/t$, t = cubet thickness (1 cm); A is a constant; E_g indicates the band gap energy; exponent n depends on the type of transition; and h denotes Planck's constant.

Equation 1 was used to plot $(\alpha h\upsilon)^2$ vs $h\upsilon$ (Figure 5) from which band gap energy (E_g) of the complexes was calculated by extrapolating the linear portion of the curve to $(\alpha h\upsilon)^2 = 0$. The band gap energy of complexes **1** and **2** were 4.1 and 2.9 eV, respectively. In the solar cell, optoelectronic, and electronic applications, this result was significant because the small band gap energy expanded the electronic progress between highest occupied molecular orbital and lowest unoccupied molecular orbital energy levels and increased the electrical conductivity of the complexes.[53−56] The band gap value suggests that complexes are semiconductor materials and complex **2** has shown photocatalytic activity due to the lower band gap energy value (2.9 eV).

Photocatalytic Activity. We continued our experiment to investigate the photocatalytic activity of the complexes against different types of organic dyes because the band gap of the complexes suggests that complexes are semiconductor materials. The photocatalytic activity of the complexes was investigated against MB, Congo red (CR), methyl orange (MO), rhodamine B (RB), and naphthalol orange (NO) in the presence of sunlight (Figure 6a). Among the two complexes, complex **2** has photocatalytic activity against MB (Figure 6b) due to lower band gap energy. The degradation rate of MB by complex **2** in

DOI: 10.1021/acsomega.9b02268
ACS Omega 2019, 4, 16068−16079

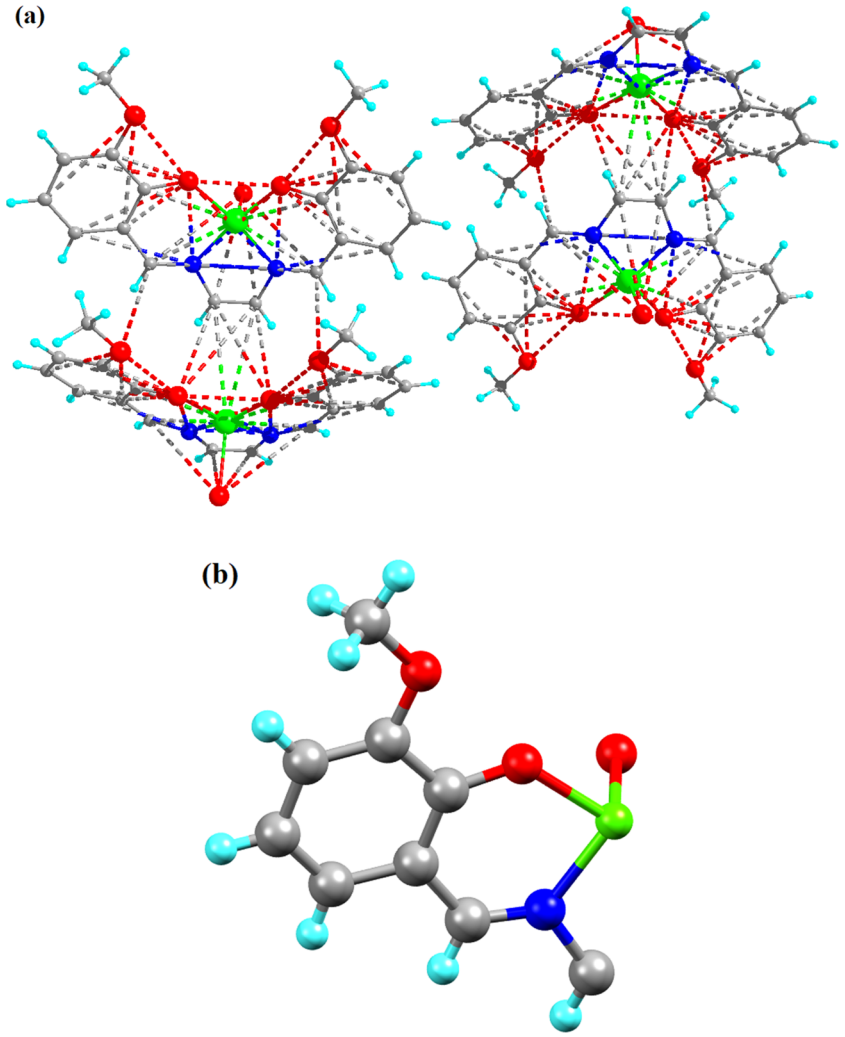

Figure 3. (a) van der Waals interaction and (b) asymmetric unit of complex **2**.

210 min was 50%. Photocatalytic degradation of MB by complex **2** follows the pseudo-first-order kinetics, and rate constant was determined by the following relation: $\ln \frac{C_o}{C} = kt$, where C_0 and C denote the MB dye concentration at times $t = 0$ and $t = t$, respectively. The inset in Figure 6b shows a good linear plot of $\ln \frac{C_o}{C}$ vs t, in which the rate constant was 5.46×10^{-5} s^{-1}.

Complex **1** has no photocatalytic activity due to higher band gap energy value, as a result of which the electron cannot make an effective transition from valence band to conduction band in the presence of sunlight. The proposed mechanistic pathway for the degradation of MB in the presence of complex **2** is shown in Figure 7.

H_2O_2 Sensing by Complexes. To detect the sensing capacity of the complexes in the presence of H_2O_2 by adding 1 mL of 20 mM H_2O_2 to 3 mL solution of the complexes, the electronic spectrum was recorded at regular intervals. Figure 8 shows that absorbance of complex **1** decreases with increasing time in the presence of H_2O_2. After 10 min, we have observed that the characteristic peak of complex **1** at 274 nm disappears and the color intensity of complex **1** turns from brown to colorless. It indicates that complex **1** has H_2O_2 decomposing ability, whereas complex **2** has no sensing ability. This function of complex **1** can be used as the measure to rapidly detect H_2O_2 in unknown samples. The addition of H_2O_2 to the Fe(III) complex results in the formation of free radicals, which initiated the degradation of iron complex, and Fe(III) gets reduced to Fe(II) and decreases the absorbance of complex **1**.

The possible reaction mechanism of H_2O_2 decomposition by complex **1** is given below.

$$H_2O_2 \underset{\text{fast}}{\overset{K_1}{\rightleftharpoons}} 2H^+ + 2HO_2^- \tag{2}$$

$$[Fe^{III}(\text{O-VEDH}_2)(H_2O)_2]^+ \underset{\text{fast}}{\overset{K_2}{\rightleftharpoons}} [Fe^{III}(\text{O-VEDH}_2)(OH)(H_2O) +][H^+] \tag{3}$$

$$[Fe^{III}(\text{O-VEDH}_2)(OH)(H_2O)] + HO_2 \underset{\text{fast}}{\overset{K_3}{\rightleftharpoons}} [Fe^{III}(\text{O-VEDH}_2)(OH)(HO_2)]^- + H_2O \tag{4}$$

$$[Fe^{III}(\text{O-VEDH}_2)(OH)(H_2O)]^- \underset{\text{slow}}{\overset{K_1}{\rightleftharpoons}} [Fe^{II}(\text{O-VEDH}_2)(OH)(HO_2^{\bullet})]^- \text{intermediate(activespecies)} \tag{5}$$

DOI: 10.1021/acsomega.9b02268
ACS Omega 2019, 4, 16068−16079

Table 4. van der Waals Interaction of Complexes 1 and 2

complex 1		complex 2	
atoms 1,2	*d* 1,2 (Å)	atoms 1,2	*d* 1,2 (Å)
N3−H6B	2.655(29)	O3−C007	3.981(62)
O8−H6B	1.919(39)	O3−C00E	3.657(117)
O8−H16A	2.647(29)	H00E−O2	3.960(36)
O6−O8	2.729(48)	H007−O2	3.395(38)
O8−H14	2.957(43)	H007−O1	3.721(31)
H7−O9	2.929(44)	C007−O2	3.664(70)
O9−H5	2.5834(36)	C00E−O1	3.482(125)
O9−H6A	2.266(48)	H00G−N1	3.477(46)
N3−6A	2.764(26)	H00G−O1	3.160(31)
O7−H6A	2.560(46)	N1−H00E	3.858(50)
O7−H6B	2.851(57)	N1−N1	2.558(70)
H4−O7	2.538(36)	N1−N00C	3.645(70)
		N1−C006	2.930(62)
		O1−N1	2.794(48)
		O1−O1	2.740(35)
		O1−O2	2.589(39)
		O2−H00D	2.649(26)
		O2−C00D	3.692(67)
		C009−O2	3.617(49)
		O1−C00B	3.614(56)
		O1−C00C	3.694(59)
		O1−C009	2.423(54)
		O1−C007	2.952(56)
		O1−H007	3.895(30)

$$[Fe^{II}(O\text{-}VEDH_2)(OH)(HO_2^{\bullet})]^- \underset{\text{fast}}{\overset{K_2}{\rightleftharpoons}} [Fe^{III}(O\text{-}VEDH_2)(OH)(O_2)]^- \quad (6)$$

$$\text{rate} = \frac{k_1\sqrt{k_1}\,k_2k_3[Fe^{III}(O\text{-}VEDH_2)(H_2O)_2]^+}{H^+} \quad (7)$$

In the possible proposed reaction mechanism, eq 5 was an intermediate of the decomposition of H_2O_2 by complex **1**.[57]

DNA Binding. Before adding CT-DNA to complexes, the stabilities of complexes **1** and **2** in Tris−HCl buffer solution were measured by a UV−visible spectrophotometer at room temperature for 1 h (each 15 min interval measured by UV) and the absorption peak was not changed. Figure 9 indicates that the UV−vis absorption spectrum of complexes **1** and **2** have absorption peak at 274 and 374 nm, respectively, which can be assigned d−d transition. To demonstrate the binding characteristics of the complexes with CT-DNA, we used electronic absorption spectroscopy through changes in absorbance and shift in wavelength. The wavelengths of complexes **1** and **2** exhibit blue shift (for complex **1**, the wavelength shifts from 274 to 274, 273, 272, 271, and 271 nm with increasing concentration of CT-DNA of 20, 40, 80, 160, and 320 μL, respectively, and similarly in complex **2**, also wavelength shifts from 374 to 371, 371, 370, 370, and 369 nm with increasing concentration of CT-DNA of 20, 40, 80, 160, and 320 μL, respectively), when the concentration of CT-DNA was increased.

The intercalability of a metal complex depended on the conjugation, planarity, ligand donor atoms, and the formation of the geometry of the complex.[25] The absorption spectra of the complex binding to DNA through intercalation reveal that blue and red shifts occur due to strong staking interaction between ligand of complexes and base pairs of DNA. The binding constant K_b of the complexes was determined by eq 8[58]

$$[\text{DNA}] \times (\varepsilon_a - \varepsilon_f)^{-1} = [\text{DNA}] \times (\varepsilon_b - \varepsilon_f)^{-1} + K_b^{-1} \times (\varepsilon_b - \varepsilon_f)^{-1} \quad (8)$$

where ε_a, ε_f, and ε_b denote extinction coefficients of the complex, CT-DNA, and bound complex, respectively. The binding constants of complexes **1** and **2** were 3.770×10^3 and 1.488×10^4 M^{-1}, respectively, as shown in Table 5. Therefore, binding constant values lie within the range of a characteristic of the CT-DNA binding by complexes through intercalative mode.[59,60]

CONCLUSIONS

The Fe(III) and Cu(II) complexes of the designed Schiff base ligand *N,N′*-bis(O-vanillinidene)ethylenediamine (O-VEDH$_2$) were successfully synthesized and characterized by single X-ray crystallography and Fourier-transform infrared (FT-IR) spectroscopy. Several applications of the metal complexes were investigated, such as MOFs, conductivity, photocatalytic activity, H_2O_2 sensing, and DNA binding activity. Complexes **1** and **2** have MOF structures and semiconductor properties, and their optical band gap energy values were 4.1 and 2.9 eV, respectively. Complex **1** has sensing ability to decompose H_2O_2, but it has no photocatalytic activity, whereas complex **2** has photocatalytic activity against MB degradation but no sensing ability to decompose H_2O_2. Both the complexes were bound to CT-DNA via intercalative mode of interaction, and binding constants were 3.770×10^3 and 1.488×10^4 M^{-1}, respectively.

EXPERIMENTAL SECTION

Materials and Methods. All chemical reagents used were commercially available and used without further purification. The solvents were used as received.

Synthesis of Schiff Base Ligand. A methanolic solution of O-Vanillin (0.608 g) was mixed with the methanolic solution of ethylenediamine (0.133 g) under constant stirring for 15 min at room temperature, resulting in the formation of a yellow precipitate. The precipitate was filtered, washed with methanol, and finally dried in vacuum. The yield of Schiff base ligand is 80% (0.486 g). ^{1}H NMR (400 MHz, $CDCl_3$) δ: 8.34 (s, 1H), 6.92 (d, J = 4 Hz, 1H), 6.87 (m, 1H), 6.82 (d, J = 8.3 Hz, 1H), 4.73 (s, J = 7.1 Hz, 1H), 3.97 (t, J = 12.1 Hz, 2H), and 3.50 (s, 3H), as shown in Figure S1 (Supporting Information). Solubility: acetonitrile, dimethyl sulfoxide, dimethylformamide (DMF). Scheme 1 presents the synthesis of Schiff base ligand *N,N′*-bis(O-vanillinidene)ethylenediamine (O-VEDH$_2$).

Scheme 1. Preparation of Schiff Base Ligand *N,N′*-Bis(O-vanillinidene)ethylenediamine (O-VEDH$_2$)

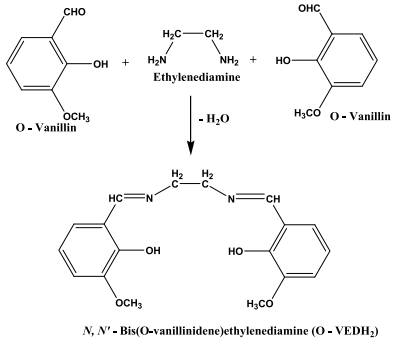

DOI: 10.1021/acsomega.9b02268
ACS Omega 2019, 4, 16068−16079

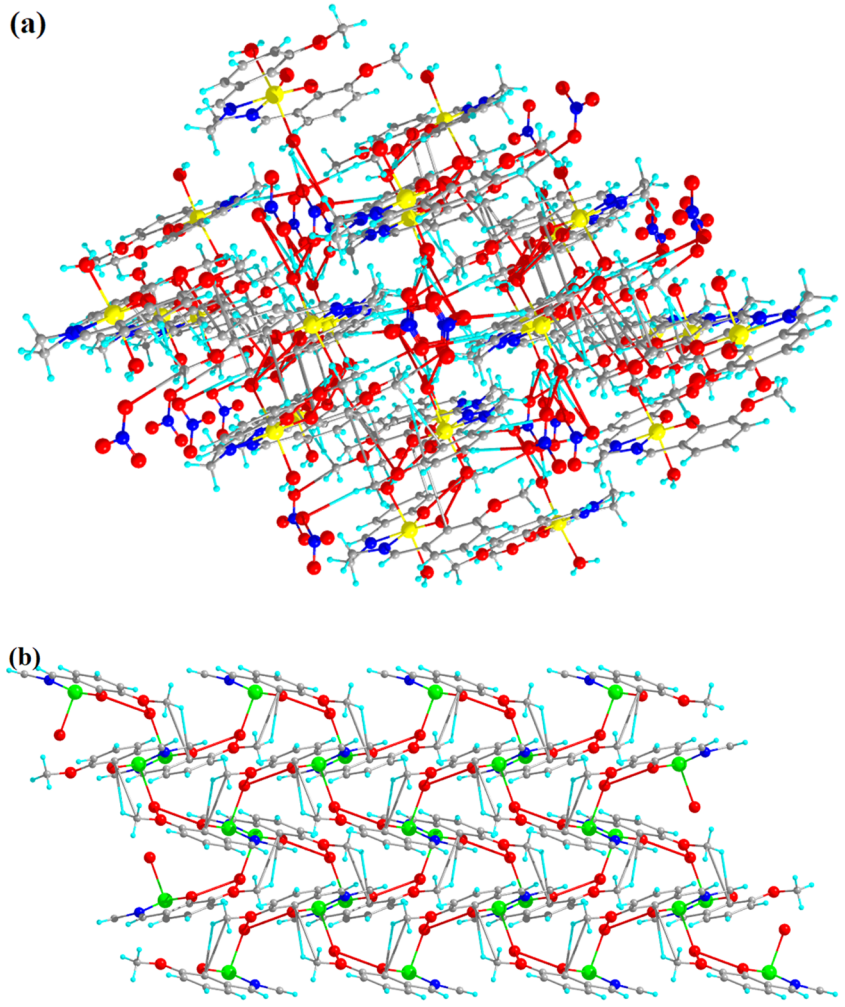

Figure 4. MOF at (010) *b* axis in central projection for (a) complex **1** and (b) complex **2**.

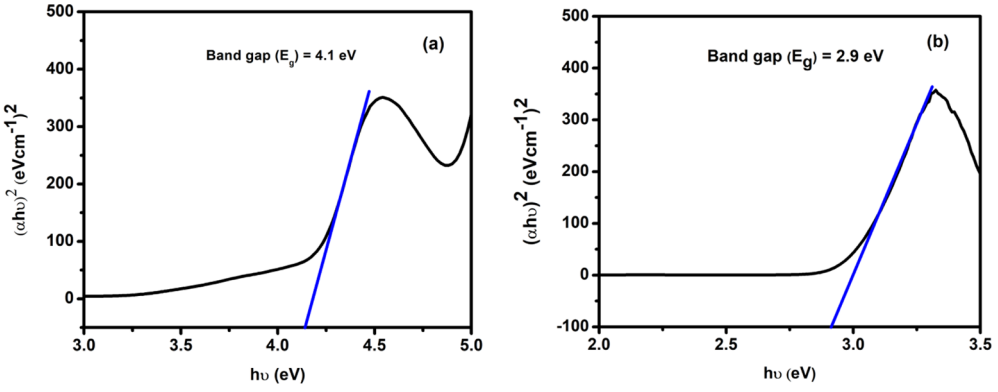

Figure 5. Band gap energies of (a) complex **1** and (b) complex **2**.

Synthesis of $[C_{18}H_{22}FeN_2O_6]NO_3$ (1). $FeCl_3$ (0.487g, 3 mmol) was dissolved in 10 mL of acetonitrile, followed by dropwise addition of O-$VEDH_2$ (0.305 g, 1 mmol) (separately soluble in MeCN solution) and stirred for another 2 h until a clear solution is obtained. Finally, the resulting solution was filtered and one part of the brown filtrate was kept for slow evaporation and another part is layered in diethyl ether. Within a week, high-quality black single crystals resulted under both conditions in high yield, which were washed with Et_2O (two to three times) and dried under vacuum. Yield: 35% (0.17 g). Anal. calcd for complex **1** $C_{18}H_{22}FeN_3O_9$: C, 45.01; H, 4.62; N, 8.75%. Found: C, 45.11; H, 4.82; N, 8.56%. Selected IR data in cm^{-1}: 633 (s), 739 (s), 1080 (m), 1218 (m), 1384 (b), 1442 (s), 1550 (s), 1618 (b) [s = strong, m = medium, b = broad] (for a detailed discussion of IR spectrum of **1**, see Figure S2a).

Synthesis of $C_{18}H_{16}CuN_2O_5$ (2). A similar method was followed for the synthesis of complex **2**. Copper sulfate (0.250 g, 1 mmol) was dissolved in 10 mL of methanol followed by dropwise addition of acetonitrile solution (0.61 g, 2 mmol) of O-$VEDH_2$ with the other conditions remaining constant. Within a

DOI: 10.1021/acsomega.9b02268
ACS Omega 2019, 4, 16068−16079

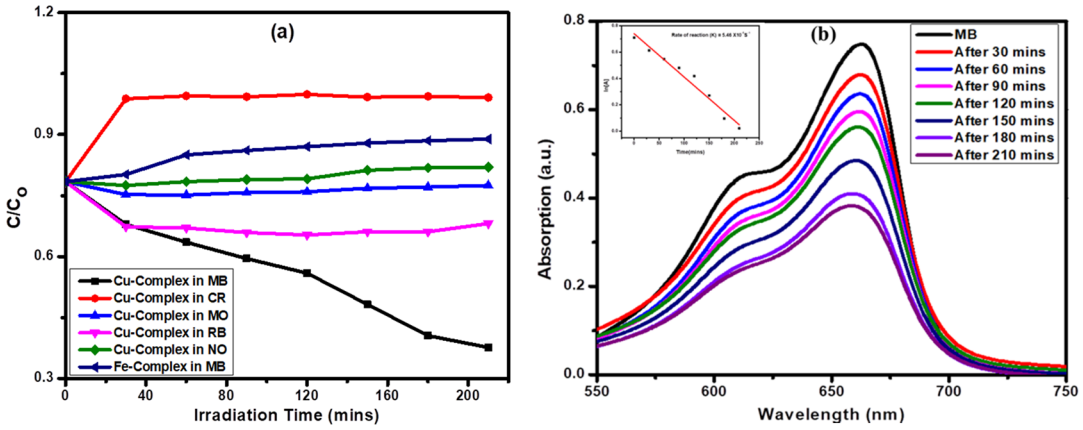

Figure 6. (a) Kinetics of the dye degradation and (b) MB degradation by complex **2** and rate of reaction.

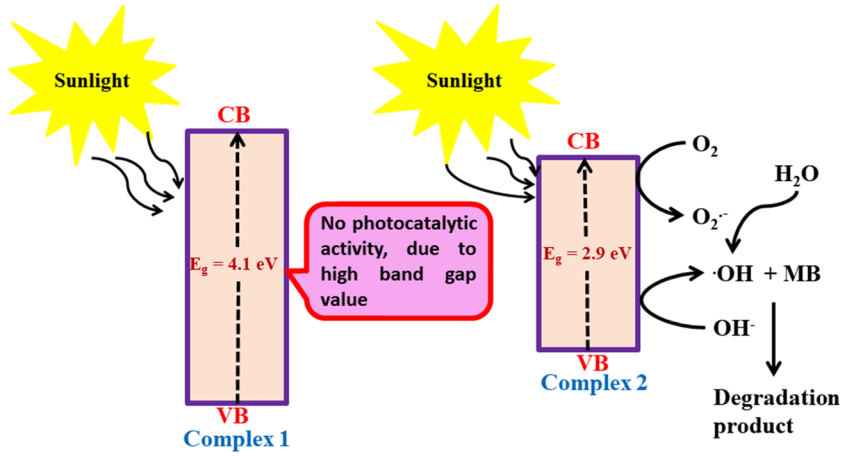

Figure 7. Possible mechanism and reason for dye degradation by complex **2** in the presence of sunlight.

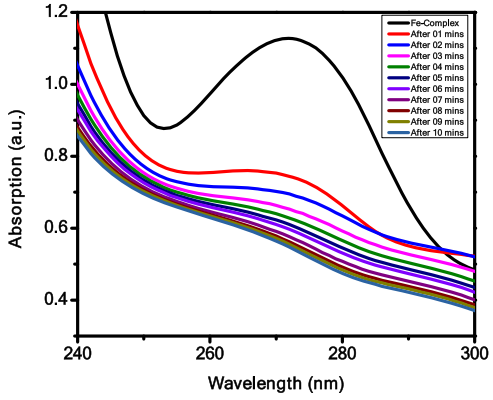

Figure 8. H_2O_2 sensing by Complex **1**.

week, high-quality green single crystals appeared, which were washed with Et_2O (two to three times) and dried under vacuum. Yield: 30% (0.075 g). Anal. calcd for complex **2** $C_{18}H_{16}CuN_2O_5$: C, 53.54; H, 3.99; N, 6.94%. Found: C, 53.23; H, 3.85; N, 6.85%. Selected IR data in cm^{-1}: 499 (b), 601 (s), 772 (s), 1080 (m), 1218 (s), 1394 (m), 1437 (s), 1544 (s), 1636 (b) [s = strong, m = medium, b = broad] (for a detailed discussion of IR spectrum of **2**, see Figure S2b).

Physical Measurements. 1H NMR spectroscopy was performed on a JEOL-400 MHz spectrometer. Infrared spectra were recorded in the solid-state (KBr pellets) using a PerkinElmer FT-IR spectrometer in the 400−4000 cm^{-1} range. Bruker SMART APEX performed elemental analysis (C, H, N) and X-ray crystallography. UV−visible spectrophotometer (Shimadzu UV-1800) was used to analyze the electronic spectrum of complexes.

Crystallographic Data Collection and Refinement. Single precious stone X-beam information from complexes **1** and **2** was collected at 293 and 99 K on the Bruker SMART APEX CCD diffractometer using SMART/SANTI programming.[61] Intensity data were collected with Mo Kα graphite monochromatized radiation (0.71073 Å) at 100 K. The structures were understood by a coordinate strategy using the SHELXS-2013[62] program, which was incorporated in WinGX.[63,64] Exact corrections to the absorption were linked to SADABS.[65] All nonhydrogen particles were refined with an anisotropic displacement coefficient. The hydrogen carbon-bonded particles were incorporated in geometric positions, and the given warm parameters are one to two times those of the molecule to which they were attached. An initial search for reciprocal space exposed that complexes **1** and **2** crystallize in monoclinic and orthorhombic space groups with *P*121/*n*1 and *Pnma*, respectively. A and B alerts are observed in the checkCIF file of the complexes due to the presence of high disorder in the structure and solvent molecules.

The results of the precious crystal data and structure-refined information of complexes **1** and **2** are available in Table 1.

Dye Degradation. Rhodamine B (RB), Congo Red (CR), methyl orange (MO), naphthalol orange (NO), and methylene blue (MB) were separately dissolved in water. The complex (10

DOI: 10.1021/acsomega.9b02268
ACS Omega 2019, 4, 16068−16079

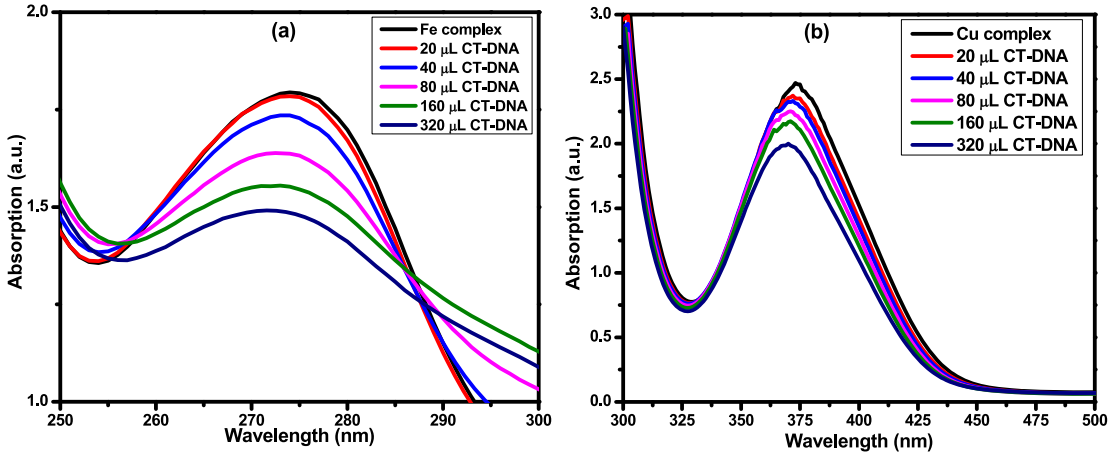

Figure 9. Absorption spectra of complexes in the absence and presence of CT-DNA: (a) complex **1** and (b) complex **2**.

Table 5. Absorption Titration Data of Complexes 1 and 2

Absorption	[DNA] / (ε_a–ε_f) × 10^6 M^2cm	[DNA] ×10^4M	K_b (M^{-1})	
		Complex 1		
1.794	0.000	0.000		
1.784	5.4017	1.194		
1.735	10.8034	2.388		
1.638	21.6068	4.776	3.770 × 10^3 M^{-1}	
1.554	43.2136	9.552		
1.491	86.4212	19.104		
		Complex 2		
2.459	0.000	0.000		
2.36	1.480	1.194		
2.321	2.96	2.388		
2.247	5.92	4.776	1.488 × 10^4 M	
2.167	11.84	9.552		
1.986	23.68	19.104		

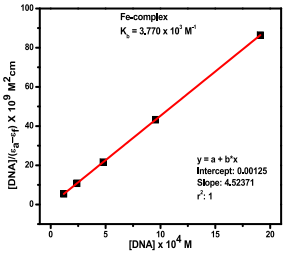

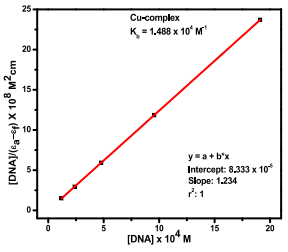

mg) was soaked in 10 mL of dye solution and kept under sunlight. Furthermore, we examined the complex's specific photocatalytic activity, and readings with UV spectroscopy were taken regularly.

Hydrogen Peroxide-Sensing Capacity of the Complexes. The detection of H_2O_2 by both complexes is investigated by the protocol developed by Bera et al. (2013).[66] Initially, complexes **1** and **2** were dissolved in CH_3CN and DMF, respectively. A suitable dilute solution of the complexes (3 mL) was noted for the initial of UV−visible spectrum. In the complex solution, 1 mL of 20 mM H_2O_2 was added. The readings were taken at regular intervals with UV−visible spectroscopy.

DNA Binding Study. Calf-thymus (CT) DNA was dissolved in Tris−HCl buffer (pH = 7.25) solution, and its purity was checked from the absorbance ratio A260/A280, which is in the range 1.8−1.9. Metal complexes **1** and **2** were dissolved, and absorption titration experiments were performed using increased concentration of CT-DNA with the constant amount with the metal complex.

■ ASSOCIATED CONTENT

Supporting Information

The Supporting Information is available free of charge on the ACS Publications website at DOI: 10.1021/acsomega.9b02268.

X-ray crystallographic data (CIF) (CIF)

^{1}H NMR of Schiff base ligand (Figure S1); FT-IR of (a) complex **1** and (b) complex **2** (Figure S2); MOF at (100)

DOI: 10.1021/acsomega.9b02268
ACS Omega 2019, 4, 16068−16079

"*a*" axis in central projection of complex **2** (Figure S3); selected geometric information of the complex **1** (Table S1); selected geometric information of the complex **2** (Table S2) (PDF)

Designed and synthesized of new *N*,*N*′-bis(O-vanillinidene)ethylenediamine (O-VEDH$_2$) Schiff base ligand; synthesis of novel [$C_{18}H_{22}FeN_2O_6$]NO_3 (**1**) and $C_{18}H_{16}CuN_2O_5$ (**2**) complex employing by O-VEDH$_2$

Accession Codes

CCDC 1937318 and 1937320 contain the supplementary crystallographic data for complexes **1** and **2**, respectively. These data are available free of charge at http://www.ccdc.cam.ac.uk/conts/retrieving.html or from the Cambridge Crystallographic Data Centre, 12 Union Road, Cambridge CB2 1EZ, U.K.; Fax: (+44) 1223-336-033; E-mail:deposit@ccdc.cam.ac.uk. Supporting Information (SI) available: Figures S1−S3 and Tables S1 and S2.

AUTHOR INFORMATION

Corresponding Author

*E-mail: tanmay.ghorai@igntu.ac.in, tanmayghorai66@gmail.com.

ORCID

Tanmay Kumar Ghorai: 0000-0001-8758-7956

Author Contributions

The Schiff base ligand and metal complexes were synthesized by M.K.G. and Dr S.P. The applications of the complexes were investigated by M.K.G. The manuscript was designed and written by M.K.G. and Dr T.K.G. All of the authors have given approval to the final version of the manuscript.

Notes

The authors declare no competing financial interest.

ACKNOWLEDGMENTS

This work was fully supported by Madhya Pradesh Council of Science & Technology, Govt. of India, Madhya Pradesh (File No. A/R&D/RP-2/ Phy & Engg./2017-18/271); Indira Gandhi National Tribal University, Amarkantak, Madhya Pradesh; and University of Gour Banga, Malda, India. The authors acknowledge IIT Indore and IACS Kolkata, Madhya Pradesh, India, for measurement of single X-ray crystallography. They also acknowledge GGU (Central University), Chhattisgarh, India, for FT-IR measurement. The authors thank Dr Hari Singh Gour University (Central University), Madhya Pradesh, India, for ^{1}H NMR measurement.

REFERENCES

(1) Vieira, A. P.; Wegermann, C. A.; Ferreira, A. M. D. C. Comparative studies of Schiff base-copper (II) and zinc (II) complexes regarding their DNA binding ability and cytotoxicity against sarcoma cells. *New J. Chem.* **2018**, *42*, 13169−13179.

(2) (a) Zhang, J.; Xu, L.; Wong, W. Y. Energy materials based on metal Schiff base complexes. *Coord. Chem. Rev.* **2018**, *355*, 180−198. (b) Rana, S.; Biswas, J. P.; Sen, A.; Clémancey, M.; Blondin, G.; Latour, J. M.; Rajaraman, G.; Maiti, D. Selective C−H halogenation over hydroxylation by non-heme iron (iv)-oxo. *Chem. Sci.* **2018**, *9*, 7843−7858.

(3) Kaczmarek, M. T.; Zabiszak, M.; Nowak, M.; Jastrzab, R. Lanthanides: Schiff base complexes, applications in cancer diagnosis, therapy, and antibacterial activity. *Coord. Chem. Rev.* **2018**, *370*, 42−54.

(4) Silva, P. P.; Guerra, W.; Silveira, J. N.; Ferreira, A. M. D. C.; Bortolotto, T.; Fischer, F. L.; Terenzi, H.; Neves, A.; Pereira-Maia, E. C. Two new ternary complexes of copper (II) with tetracycline or doxycycline and 1, 10-phenanthroline and their potential as antitumoral: cytotoxicity and DNA cleavage. *Inorg. Chem.* **2011**, *50*, 6414−6424.

(5) Al Zoubi, W.; Ko, Y. G. Organometallic complexes of Schiff bases: Recent progress in oxidation catalysis. *J. Organomet. Chem.* **2016**, *822*, 173−188.

(6) Matsunaga, S.; Shibasaki, M. Multimetallic schiff base complexes as cooperative asymmetric catalysts. *Synthesis* **2013**, *45*, 421−437.

(7) Silva, P. P.; Guerra, W.; dos Santos, G. C.; Fernandes, N. G.; Silveira, J. N.; da Costa Ferreira, A. M.; Bortolotto, T.; Terenzi, H.; Bortoluzzi, A. J.; Neves, A.; Pereira-Maia, E. C. Correlation between DNA interactions and cytotoxic activity of four new ternary compounds of copper (II) with N-donor heterocyclic ligands. *J. Inorg. Biochem.* **2014**, *132*, 67−76.

(8) Cozzi, P. G. Metal−Salen Schiff base complexes in catalysis: practical aspects. *Chem. Soc. Rev.* **2004**, *33*, 410−421.

(9) Gupta, K. C.; Sutar, A. K. Catalytic activities of Schiff base transition metal complexes. *Coord. Chem. Rev.* **2008**, *252*, 1420−1450.

(10) Matsunaga, S.; Shibasaki, M. Recent advances in cooperative bimetallic asymmetric catalysis: dinuclear Schiff base complexes. *Chem. Commun.* **2014**, *50*, 1044−1057.

(11) Yang, J.; Shi, R.; Zhou, P.; Qiu, Q.; Li, H. Asymmetric Schiff bases derived from diaminomaleonitrile and their metal complexes. *J. Mol. Struct.* **2016**, *1106*, 242−258.

(12) Kostova, I.; Saso, L. Advances in research of Schiff-base metal complexes as potent antioxidants. *Curr. Med. Chem.* **2013**, *20*, 4609−4632.

(13) Erxleben, A. Transition metal salen complexes in bioinorganic and medicinal chemistry. *Inorg. Chim. Acta.* **2018**, *472*, 40−57.

(14) Lee, S. J.; Lee, S. W. Cd (II), Ni (II), and Co (II) complexes based on a pyridyl−amine Schiff-base ligand:[M (L) 2 (NO3)]·(NO3)(M= Cd, Ni, Co), cis-[CoL2Cl2]·(C6H6), and [Co (L) 3]·(ClO4) 2 (CH3CN) 2 (H2O)(L = N-(2-pyridylmethylene) benzene-1, 4-diamine,(2-py) CHNC6H4NH2). *Polyhedron* **2019**, *159*, 259−264.

(15) Liu, Y. H.; Li, A.; Shao, J.; Xie, C. Z.; Song, X. Q.; Bao, W. G.; Xu, J. Y. Four Cu (II) complexes based on antitumor chelators: Synthesis, structure, DNA binding/damage, HSA interaction and enhanced cytotoxicity. *Dalton Trans.* **2016**, *45*, 8036−8049.

(16) Mollick, S.; Mandal, T. N.; Jana, A.; Fajal, S.; Desai, A. V.; Ghosh, S. K. Ultrastable Luminescent Hybrid Bromide Perovskite@MOF Nanocomposites for the Degradation of Organic Pollutants in Water. *ACS Appl. Nano Mater.* **2019**, No. 2214.

(17) Cheng, R.; Ou, S.; Xiang, B.; Li, Y.; Liao, Q. Equilibrium and molecular mechanism of anionic dyes adsorption onto copper (II) complex of dithiocarbamate-modified starch. *Langmuir* **2009**, *26*, 752−758.

(18) Xiao, J. D.; Jiang, H. L. Metal−Organic Frameworks for Photocatalysis and Photothermal Catalysis. *Acc. Chem. Res.* **2018**, No. 521.

(19) Naskar, K.; Dey, A.; Maity, S.; Bhunia, M. K.; Ray, P. P.; Sinha, C. Novel Porous Polycatenated Iodo-Cadmium Coordination Polymer for Iodine Sorption and Electrical Conductivity Measurement. *Cryst. Growth Des.* **2019**, No. 1806.

(20) Du, M.; Li, L.; Li, M.; Si, R. Adsorption mechanism on metal organic frameworks of Cu-BTC, Fe-BTC and ZIF-8 for CO_2 capture investigated by X-ray absorption fine structure. *RSC Adv.* **2016**, *6*, 62705−62716.

(21) Yang, J.; Zhao, F.; Zeng, B. One-step synthesis of a copper-based metal−organic framework−graphene nanocomposite with enhanced electrocatalytic activity. *RSC Adv.* **2015**, *5*, 22060−22065.

(22) Rajalakshmi, S.; Kiran, M. S.; Nair, B. U. DNA condensation by copper (II) complexes and their anti-proliferative effect on cancerous and normal fibroblast cells. *Eur. J. Med. Chem.* **2014**, *80*, 393−406.

(23) Torres, J. F.; Macias, M. A.; Franco-Ulloa, S.; Miscione, G. P.; Cobo, J.; Hurtado, J. Cu (II) and Zn (II) Complexes with Dinitrobenzoates and Pyrazolyl Ligands: Structural and Thermal Stability Influence of NH Moiety. *Cryst. Growth Des.* **2019**, No. 246.

DOI: 10.1021/acsomega.9b02268
ACS Omega 2019, 4, 16068−16079

(24) Wu, M. Z.; Shi, J. Y.; Chen, P. Y.; Tian, L.; Chen, J. Two 3D Cobalt (II) Metal−Organic Frameworks with Micropores for Selective Dye Adsorption. *Inorg. Chem.* **2019**, *58*, 3130−3136.
(25) Tanaka, S.; Sato, H.; Ishida, Y.; Deng, Y.; Haraguchi, T.; Akitsu, T.; Sugiyama, M.; Hara, M.; Moon, D. Photo-Control of Adsorption of Dye Metal Complexes Incorporating Chiral Schiff Base Ligands Containing Azo-Groups on TiO2. *J. Korean Chem. Soc.* **2018**, *62*, 328−332.
(26) Wen, T.; Zhang, D. X.; Zhang, J. Two-dimensional copper (I) coordination polymer materials as photocatalysts for the degradation of organic dyes. *Inorg. Chem.* **2013**, *52*, 12−14.
(27) Beheshti, A.; Fard, E. S. M.; Kubicki, M.; Mayer, P.; Abrahams, C. T.; Razatofighi, S. E. Design, synthesis and characterization of copper-based coordination compounds with bidentate (N, N and N, O) ligands: reversible uptake of iodine, dye adsorption and assessment of their antibacterial properties. *CrystEngComm* **2019**, *21*, 251−262.
(28) Yue, C.-Y.; Lei, X.-W.; Han, Y.-F.; Lu, X.-X.; Tian, Y.-W.; Xu, J.; Liu, X.-F.; Xu, X. Transition-Metal-Complex Cationic Dyes Photosensitive to Two Types of 2D Layered Silver Bromides with Visible-Light-Driven Photocatalytic Properties. *Inorg. Chem.* **2016**, *55*, 12193−12203.
(29) Pathak, S.; Ghosh, M. K.; Ghorai, T. K. Luminescence, Dye Degradation and DNA Binding Properties of a Dinuclear Nona-Coordinated Y (III) Complex. *ChemistrySelect* **2018**, *3*, 13501−13506.
(30) Umamaheswari, C.; Lakshmanan, A.; Nagarajan, N. S. Green synthesis, characterization and catalytic degradation studies of gold nanoparticles against congo red and methyl orange. *J. Photochem. Photobiol., B* **2018**, *178*, 33−39.
(31) Yang, L.; Li, X.; Sun, C. Y.; Wu, H.; Wang, C. G.; Su, Z. M. A stable pillared-layer Cu (ii) metal−organic framework with magnetic properties for dye adsorption and separation. *New J. Chem.* **2017**, *41*, 3661−3666.
(32) Winterbourn, C. C. Reconciling the chemistry and biology of reactive oxygen species. *Nat. Chem. Biol.* **2008**, *4*, No. 278.
(33) Mukhopadhyay, D.; Dasgupta, P.; Roy, D. S.; Palchoudhuri, S.; Chatterjee, I.; Ali, S.; Dastidar, S. G. A Sensitive In vitro Spectrophotometric Hydrogen Peroxide Scavenging Assay using 1, 10-Phenanthroline. *Free Rad. Antiox.* **2016**, *6*, 124−132.
(34) Dröge, W. Free radicals in the physiological control of cell function. *Physiol. Rev.* **2002**, *82*, 47−95.
(35) Liu, R.; Wei, Y.; Zheng, J.; Zhang, H.; Sheng, Q. A hydrogen peroxide sensor based on silver nanoparticles biosynthesized by Bacillus subtilis. *Chin. J. Chem.* **2013**, *31*, 1519−1525.
(36) Tredwin, C. J.; Naik, S.; Lewis, N. J.; Scully, C. B. E. C. Hydrogen peroxide tooth-whitening (bleaching) products: review of adverse effects and safety issues. *Br. Dent. J.* **2006**, *200*, 371−376.
(37) Zeng, L.; Miller, E. W.; Pralle, A.; Isacoff, E. Y.; Chang, C. J. A selective turn-on fluorescent sensor for imaging copper in living cells. *J. Am. Chem. Soc.* **2006**, *128*, 10−11.
(38) Lustig, W. P.; Mukherjee, S.; Rudd, N. D.; Desai, A. V.; Li, J.; Ghosh, S. K. Metal−organic frameworks: functional luminescent and photonic materials for sensing applications. *Chem. Soc. Rev.* **2017**, *46*, 3242−3285.
(39) Yu, Y.; Ma, J. P.; Zhao, C. W.; Yang, J.; Zhang, X. M.; Liu, Q. K.; Dong, Y. B. Copper (I) metal−organic framework: visual sensor for detecting small polar aliphatic volatile organic compounds. *Inorg. Chem.* **2015**, *54*, 11590−11592.
(40) Wang, D.; Wang, M.; Li, Z. Fe-based metal−organic frameworks for highly selective photocatalytic benzene hydroxylation to phenol. *ACS Catal.* **2015**, *5*, 6852−6857.
(41) Kreno, L. E.; Leong, K.; Farha, O. K.; Allendorf, M.; Van Duyne, R. P.; Hupp, J. T. Metal−organic framework materials as chemical sensors. *Chem. Rev.* **2011**, *112*, 1105−1125.
(42) Hemmert, C.; Pitié, M.; Renz, M.; Gornitzka, H.; Soulet, S.; Meunier, B. Preparation, characterization and crystal structures of manganese (II), iron (III) and copper (II) complexes of the bis [di-1, 1-(2-pyridyl) ethyl] amine (BDPEA) ligand; evaluation of their DNA cleavage activities. *J. Biol. Inorg. Chem.* **2001**, *6*, 14−22.
(43) Wang, J.; Liu, X.; Sun, Y.; Yan, L.; He, S. Synthesis, crystal structures, thermal properties, and DNA-binding studies of transition metal complexes with imidazole ligands. *J. Coord. Chem.* **2011**, *64*, 1554−1565.
(44) Zuber, G.; Quada, J. C.; Hecht, S. M. Sequence selective cleavage of a DNA octanucleotide by chlorinated bithiazoles and bleomycins. *J. Am. Chem. Soc.* **1998**, *120*, 9368−9369.
(45) Pages, B. J.; Ang, D. L.; Wright, E. P.; Aldrich-Wright, J. R. Metal complex interactions with DNA. *Dalton Trans.* **2015**, *44*, 3505−3526.
(46) Pathak, S.; Ghosh, M. K.; Mandal, M.; Mandal, V.; Bhattacharyya, A.; Ghorai, T. K. Synthesis of a new acetate bridged Cu (ii) building block generated 1D polymer and studies on structural, magnetic, antibacterial and anticancer properties. *New J. Chem.* **2019**, *43*, 2019−2029.
(47) Santini, C.; Pellei, M.; Gandin, V.; Porchia, M.; Tisato, F.; Marzano, C. Advances in copper complexes as anticancer agents. *Chem. Rev.* **2013**, *114*, 815−862.
(48) Viqueira, J.; Durán, M. L.; García-Vázquez, J. A.; Castro, J.; Platas-Iglesias, C.; Esteban-Gómez, D.; Alzuet-Piña, G.; Moldes, A.; Nascimento, O. R. Modulating the DNA cleavage ability of copper (ii) Schiff bases through ternary complex formation. *New J. Chem.* **2018**, *42*, 15170−15183.
(49) García-Ramos, J. C.; Vértiz-Serrano, G.; Macías-Rosales, L.; Galindo-Murillo, R.; Toledano-Magaña, Y.; Bernal, J. P.; Cortés-Guzmán, F.; Ruiz-Azuara, L. Isomeric Effect on the Pharmacokinetic Behavior of Anticancer CuII Mixed Chelate Complexes: Experimental and Theoretical Approach. *Eur. J. Inorg. Chem.* **2017**, *2017*, 1728−1736.
(50) Chen, W.; Wu, C. Synthesis, functionalization, and applications of metal−organic frameworks in biomedicine. *Dalton Trans.* **2018**, *47*, 2114−2133.
(51) Rojas, S.; Devic, T.; Horcajada, P. Metal organic frameworks based on bioactive components. *J. Mater. Chem. B* **2017**, *5*, 2560−2573.
(52) Brown, I. D.; Altermatt, D. Bond-valence parameters obtained from a systematic analysis of the inorganic crystal structure database. *Acta Crystallogr., Sect. B: Struct. Sci.* **1985**, *41*, 244−247.
(53) Ahmed, A. H.; Hassan, A. M.; Gumaa, H. A.; Mohamed, B. H.; Eraky, A. M.; Omran, A. A. Copper (II)-oxaloyldihydrazone complexes: Physico-chemical studies: Energy band gap and inhibition evaluation of free oxaloyldihydrazones toward the corrosion of copper metal in acidic medium. *Arab. J. Chem.* **2016**, No. 15.
(54) Turan, N.; Gündüz, B.; Körkoca, H.; Adigüzel, R.; Çolak, N.; Buldurun, K. Study of structure and spectral characteristics of the Zinc (II) and Copper (II) complexes with 5, 5-Dimethyl-2-(2-(3-nitrophenyl) hydrazono) cyclohexane-1, 3-dione and their effects on optical properties and the developing of the energy band gap and investigation of antibacterial activity. *J. Mex. Chem. Soc.* **2014**, *58*, 65−75.
(55) Sengupta, S. K.; Pandey, O. P.; Srivastava, B. K.; Sharma, V. K. Synthesis, structural and biochemical aspects of titanocene and zirconocene chelates of acetylferrocenyl thiosemicarbazones. *Transition Met. Chem.* **1998**, *23*, 349−353.
(56) Fu, M. L.; Guo, G. C.; Liu, X.; Liu, B.; Cai, L. Z.; Huang, J. S. Syntheses, structures and properties of three selenoarsenates templated by transition metal complexes. *Inorg. Chem. Commun.* **2005**, *8*, 18−21.
(57) Chi, G. T.; Nagy, Z. K.; Huddersman, K. D. Kinetic modelling of the Fenton-like oxidation of maleic acid using a heterogeneous modified polyacrylonitrile (PAN) catalyst. *Prog. React. Kinet. Mech.* **2011**, *36*, 189−214.
(58) Wolfe, A.; Shimer, G. H., Jr; Meehan, T. Polycyclic aromatic hydrocarbons physically intercalate into duplex regions of denatured DNA. *Biochemistry* **1987**, *26*, 6392−6396.
(59) Martins, D. A.; Gouvea, L. R.; Batista, D. D. G. J.; Da Silva, P. B.; Louro, S. R.; Maria de Nazaré, C. S.; Teixeira, L. R. Copper (II)−fluoroquinolone complexes with anti-Trypanosoma cruzi activity and DNA binding ability. *BioMetals* **2012**, *25*, 951−960.
(60) Patel, M. N.; Gandhi, D. S.; Parmar, P. A. Synthesis, biological aspects and SOD mimic activity of square pyramidal copper (II) complexes with the 3rd generation quinolone drug sparfloxacin and phenanthroline derivatives. *Inorg. Chem. Commun.* **2011**, *14*, 128−132.

DOI: 10.1021/acsomega.9b02268
ACS Omega 2019, 4, 16068−16079

(61) Sheldrick, G. M. *Acta Crystallogr., Sect. A: Found. Crystallogr.* **2008**, *64*, No. 112.
(62) Sheldrick, G. M. *SHELXL2013*; University of Göttingen: Germany, 2013.
(63) Farrugia, L. J. WinGX and ORTEP for Windows: an update. *J. Appl. Crystallogr.* **2012**, *45*, 849−854.
(64) Farrugia, L. J. *WinGX*, version 3; Department of Chemistry, University of Glasgow: Glasgow, Scotland, 2013.
(65) Sheldrick, G. M. *SADABS*; University of Göttingen: Göttingen, Germany, 1999.
(66) Bera, R. K.; Raj, C. R. A facile photochemical route for the synthesis of triangular Ag nanoplates and colorimetric sensing of H2O2. *J. Photochem. Photobiol., A* **2013**, *270*, 1−6.

DOI: 10.1021/acsomega.9b02268
ACS Omega 2019, 4, 16068−16079